

Snowpack dynamics in the Lebanese mountains from quasi-dynamically downscaled ERA5 reanalysis updated by assimilating remotely-sensed fractional snow-covered area

5 Esteban Alonso-González¹, Ethan Gutmann², Kristoffer Aalstad³, Abbas Fayad⁴, Marine Bouchet⁵, Simon Gascoin⁵

1- Instituto Pirenaico de Ecología, Spanish Research Council (IPE-CSIC), Zaragoza, Spain

2- Research Application Laboratory, National Center for Atmospheric Research (RAL-NCAR), Boulder, CO, United States

10 3- Department of Geosciences, University of Oslo, Oslo, Norway

4- Centre for Hydrology, University of Saskatchewan, Saskatoon, Saskatchewan, Canada

5- Centre d'Etudes Spatiales de la Biosphère (CESBIO), UPS/CNRS/IRD/INRA/CNES, Toulouse, France

Abstract: The snowpack over the Mediterranean mountains constitutes a key water resource for the downstream populations. However, its dynamics have not been studied in detail yet in many areas, mostly because of the scarcity of snowpack observations. In this work, we present a characterization of the snowpack over the two mountain ranges of Lebanon. To obtain the necessary snowpack information, we have developed a 1 km regional scale snow reanalysis (ICAR_assim) covering the period 2010-2017. ICAR_assim was developed by means of ensemble-based data assimilation of MODIS fractional snow-covered area (fSCA) through an energy and mass snow balance model the Flexible Snow Model (FSM2), using the Particle Batch Smoother (PBS). The meteorological forcing data was obtained by a regional atmospheric simulation from the Intermediate Complexity Atmospheric Research model (ICAR) nested inside a coarser regional simulation from the Weather Research and Forecasting model (WRF). The boundary and initial conditions of WRF were provided by the ERA5 atmospheric reanalysis. ICAR_assim showed very good agreement with MODIS gap-filled snow products, with a spatial correlation of $R = 0.98$ in the snow probability ($P(\text{snow})$), and a temporal correlation of $R = 0.88$ in the day of peak snow water equivalent (SWE). Similarly, ICAR_assim has shown a correlation with the seasonal mean SWE of $R = 0.75$ compared with in-situ observations from Automatic Weather Stations (AWS). The results highlight the high temporal variability of the snowpack in the Lebanon ranges, with differences between Mount Lebanon and Anti-Lebanon that cannot only be explained by hypsography with Anti-Lebanon in the rain shadow of Mount Lebanon. The maximum fresh water stored in the snowpack is in the middle elevations approximately between 2200 and 2500 m a.s.l. Thus, the resilience to further warming is low for the snow water resources of Lebanon due to the proximity of the snowpack to the zero isotherm.

Keywords — Snow, dynamical downscaling, data assimilation, fractional snow cover, Mediterranean mountains

1. Introduction

40 The hydrological processes related to mountain areas are essential for the water supplies
to a large part of humanity (Viviroli et al., 2007). Despite the relatively mild temperature
of the Mediterranean climates, mountains there often exhibit deep and long-lasting
snowpacks accumulating more than 3 meters and an average snow season of 5 months at
45 the summit areas (Alonso-González et al., 2020; Fayad et al., 2017b). Thus, as most of
the annual precipitations falls during winter season (García-Ruiz et al., 2011) the
mountain snowpack strongly reshapes the hydrographs to sustain high flows until the end
of the spring, permitting better synchronization of water demand and availability during
the dry season (García-Ruiz et al., 2011). Mediterranean snowpacks are characterized by
50 a high interannual variability, which affect the amount and seasonality of river flows
(López-Moreno and García-Ruiz 2004). Despite this variability, the thickness and high
density exhibited by the snowpack in the Mediterranean climate (Fayad et al., 2017b),
makes them an effective water storage system. In addition, high sublimation rates are
associated with Mediterranean snowpacks (Fayad and Gascoin, 2020; Herrero et al.,
2016; Schulz and de Jong, 2004). The fact that snowpack conditions are close to
55 isothermal during most of the snow season makes them highly sensitive to the current
climate warming (Alonso-González et al., 2020a; López-Moreno et al., 2017; Yilmaz et
al., 2019).

The Lebanon mountains are a clear example of Mediterranean mountains, where snow
exerts a key control on the hydrology and water resources are critically dependent on the
60 interannual fluctuations of the snowpack (El-Fadel et al., 2000). Despite their importance,
snow observations in the region are scarce (Fayad et al., 2017a), making the study of
distributed snow dynamics challenging. Recently, Fayad and Gascoin (2020) have
developed distributed snowpack simulations over key areas of Mount Lebanon, forcing the
model by interpolating observations of the few existing Automatic Weather Stations
65 (AWS) using the SnowModel by Liston and Elder (2006). They showed the importance
of the liquid water percolation scheme given the isothermal condition of the snowpack
and estimated the snow water equivalent over three key catchments in the windward
western divide of Mount Lebanon. However, due to the lack of meteorological data
outside this area, these simulations did not cover the whole mountain area of the country
70 and were limited to three snow seasons.

Remote sensing and numerical modeling have become reliable tools to generate useful
meteorological information for mountain regions (Lundquist et al., 2019), and also to
generate robust snow data worldwide. Atmospheric reanalyses are a valuable source of
long term (multidecadal) climatological information, especially at planetary scales (e.g.
75 Wegmann et al., 2017; Wu et al., 2018). However, spatially downscaling such products is
mandatory to derive relevant snow information over complex terrain (Baba et al., 2018b;
Mernild et al., 2017 among others). Dynamical downscaling has been shown to
outperform statistically gridded products for meteorological variables in complex terrain
(Gutmann et al., 2012). More specifically, high resolution fully dynamical meteorological

80 models can reproduce the snowfall patterns over complex terrain (Ikeda et al., 2010;
Rasmussen et al., 2011). However, the computational cost of full dynamical downscaling
solutions becomes prohibitive for large domains at high spatial resolutions. To reduce the
computational cost, different solutions of varying complexity have been developed using
85 statistical interpolations corrected with the topography or using simplifications of the
atmospheric dynamics (Fiddes and Gruber, 2014; Gutmann et al., 2016; Liston and Elder,
2006). In this way, energy and mass balance snowpack models have been coupled with
atmospheric models to develop multidecadal snow simulations (Alonso-González et al.,
2018; van Pelt et al., 2016 among others). In addition, remote sensing products have been
90 widely used to study the duration and variability of the snow cover (Gascoin et al., 2015;
Saavedra et al., 2017; Yilmaz et al., 2019). Assimilation of remotely sensed snow cover
observations has shown considerable potential for improving numerical snowpack
models outputs in both distributed (e.g. Baba et al., 2018; Margulis et al., 2016) and semi
distributed simulations (Cluzet et al., 2020; Fiddes et al., 2019). These approaches are
particularly promising in data-scarce regions to reduce the biases in atmospheric forcing.

95 In this work, we have simulated the snowpack of the Lebanon mountains, as an
alternative to sparse snowpack observations. We have generated a 1 km resolution
snowpack reanalysis, using an ensemble based assimilation of fractional snow-covered
area (fSCA) obtained from the Moderate Resolution Imaging Spectroradiometer
(MODIS) satellite sensor. More specifically, the ERA5 reanalysis (Hersbach, 2016) was
100 dynamically downscaled using regional atmospheric models in two steps. First, a 10 km
resolution atmospheric simulation using the Weather Research and Forecast model
(WRF) (Skamarock et al., 2008) was performed covering the period between 2010 and
2017. Then, a finer 1 km simulation using the Intermediate Complexity Atmospheric
Research model (ICAR) (Gutmann et al., 2016) was nested inside the previous WRF
105 simulation covering the same time period. To improve the ICAR snowpack outputs, the
simulated meteorological data was used to force an energy and mass balance snowpack
model, the Flexible Snow Model (FSM2) (Essery, 2015), while perturbing the
meteorological fields to generate an ensemble of snowpack simulations. Then, the
Particle Batch Smother (PBS) (Margulis et al., 2015), a Bayesian data assimilation
110 scheme, was applied to assimilate daily remotely sensed fSCA information. We tested the
generated snow products in the mountains of Lebanon with independent observations.
Finally, the dynamics of the snowpack in the mountains of Lebanon are studied from the
generated multi-year snow time series. The objectives of this paper are: i) to explore the
potential of a methodology to develop a snowpack reanalysis over data scarce regions
115 and ii) to describe the main snowpack dynamics over the Lebanese mountains. This is the
first use of ICAR for generating a snow reanalysis.

2. Study area

Lebanon is a country located on the eastern Mediterranean Sea between latitudes 33° and 35° N. Its climatology typically Mediterranean (Peel et al., 2007) influenced mainly by

120 its proximity to the Mediterranean Sea and its complex topography (Figure 1). There are
two main mountain ranges that run in parallel to the Mediterranean coast from North to
South. These mountain ranges are the Mount Lebanon and Anti-Lebanon mountains,
reaching 3088 m a.s.l. (Qurnat as Sawdā peak) and 2814 m a.s.l. (Mount Hermon peak)
respectively. The Lebanese mountains are highly karstified encouraging the infiltration of
125 rainfall and snowmelt. The land cover is mostly composed of bare rocks and soils with
irregularly distributed patches of shrubland, as well as oaks and pine forest.

Despite Lebanon having more available water resources than its neighboring countries, it
is considered a water scarce region (El-Fadel et al., 2000), where droughts are frequent
and are expected to increase due to climate change (Farajalla et al., 2011). The particular
130 spatial distribution of its mountain ranges constitutes an effective topographical barrier to
humidity advected from the Mediterranean sea, enhancing the winter precipitation as a
consequence of orographic effects (Jomaa et al., 2019). In these mountain ranges, the
combined effects of orography and Mediterranean climate results in yearly seasonal-
snowpack over a large part of the country (Mhawej et al., 2014).

135 It was estimated from satellite retrievals of snow cover that 31% of the spring discharge
of Lebanon is associated with snowmelt (Telesca et al., 2014). In addition, the
groundwater dynamics of Lebanon are mainly controlled by the snow melt as
consequence of its karstic nature (Bakalowicz et al., 2008; El-Fadel et al., 2000). Thus,
the water resource provided by the snowpack is crucial for the Lebanese society with this
140 need becoming more acute during the recent drought in the Eastern Mediterranean (Cook
et al., 2016). In addition, the water stress increased notably in recent years partially due to
the increase in domestic water demand, agricultural water use, and the Syrian refugee
crisis (Jaafar et al., 2020) but also due to the poor management of the water resources,
and water pollution.

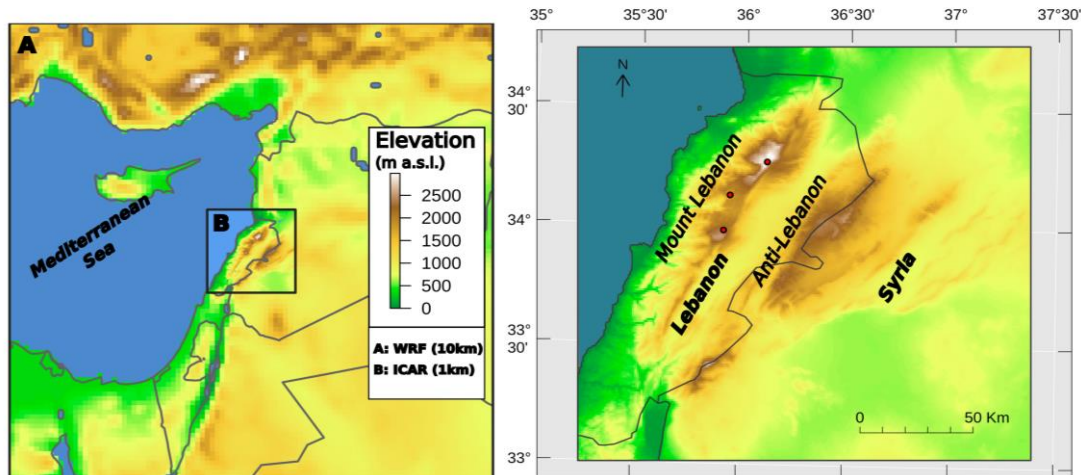


Figure 1: Atmospheric models domain configuration (left) and Lebanon Localization map (right). The red dots represent the AWS positions.

145

3. Data and Methods

3.1 Regional atmospheric simulations configuration

To generate the meteorological forcing, we used the ICAR atmospheric model nested inside a WRF simulation forced by the ERA5 reanalysis. The WRF model was used to generate a regional atmospheric simulation on a 10 km x 10 km grid, covering the eastern part of the Mediterranean Sea with 179 x 179 grid cells, centered over Lebanon's mountains (Figure 1). In the vertical dimension, the domain was composed of 35 levels with the top set to 50 hPa, similarly to other studies over Mediterranean regions (Arasa et al., 2016). The simulation covers the period from 01st of January 2010 to 30th of June 2017, using the first 9 months as spin-up period allowing for physical equilibrium between the external forcings and the land model (Montavez et al., 2017). We used the ERA5 reanalysis dataset at an hourly frequency as boundary and initial conditions of the WRF (3.8 version) model. The ERA5 dataset is an atmospheric reanalysis, which replaces the widely used ERA-Interim reanalysis (Berrisford et al., 2009). It has a spatial resolution of 30 km with 138 vertical levels with the top at 80 km. It has been shown to out perform ERA-interim in many climatological applications and as a forcing dataset for different modeling applications (Albergel et al., 2018; Tarek et al., 2019; Wang et al., 2019 among others). The parametrization schemes used in the WRF simulation include: the Thompson cloud microphysics scheme (Thompson et al., 2008), the NCAR Community Atmosphere Model (CAM) scheme for both shortwave and longwave radiations (Neale et al., 2004), the Noah-MP scheme for the land surface physics (Niu et al., 2011), the Mellor-Yamada-Janjic scheme for the planetary boundary layer (Janjic,

2002) and the Betts-Miller-Janjic scheme (Betts and Miller, 1986; Janjic, 1994) for deep and shallow convection. This WRF configuration has shown its consistency in previous studies simulating the seasonal snowpack over complex terrain (Ikeda et al., 2010; Rasmussen et al., 2011). In addition to the described parametrization, we applied the spectral nudging technique to satisfy the large scale atmospheric conditions at the higher altitudes, while allowing the model to have its own dynamics inside the planetary boundary layer (Von Storch et al., 2000; Waldron et al., 1996). The spectral nudging technique was applied for the wind vectors, temperature and geopotential with a wave number of one in each direction, based on the parameters recommended by Gómez and Miguez-Macho (2017), and nudging the waves above ~ 1000 km wavelength.

Next, the ICAR model was used to obtain a finer 1 km x 1 km spatial grid atmospheric simulation nested in the aforementioned WRF simulation domain. This enabled us to significantly reduce the high computational cost compared to a long-term high-resolution WRF simulation. ICAR is a 4D meso-atmospheric model designed for downscaling purposes based on linear mountain wave theory. The linear theory allows ICAR to compute the main dynamical effect of topography on the atmosphere using an analytical solution, thus avoiding the need to solve the Navier-Stokes equations and reducing computational cost by a factor of 100. The center of the ICAR simulation was established in the center of the WRF simulation, using 179 x 179 grid cells in both latitude and longitude directions and preventing the boundaries from intersecting complex terrain. The model top was situated at 4150 m above the topography with 12 vertical levels, using the default model levels heights (Horak et al., 2019). The model configuration used: the Thompson cloud microphysics scheme (Thompson et al., 2008), the Noah land surface model (Chen and Dudhia, 2001) and the Multidimensional Positive Definite Advection Transport Algorithm (MPDATA) for the advection (Smolarkiewicz and Margolin, 1998). Convection schemes were not implemented for this simulation and the radiative fluxes at the surface were prescribed by WRF. The lack of convection could have some impact on the total amount of precipitation, and therefore on the seasonal snowpack. However, such deviations in the total amount of precipitation are partly compensated by the PBS (as described in section 3.3.2).

3.2 Ensemble-based fractional snow cover assimilation

3.2.1 MODIS fractional snow cover area data estimation

For this study, we used satellite observations of fSCA, assimilated in an ensemble of snow simulations to improve the snow water equivalent products (SWE) of ICAR. The daily fSCA information was obtained by means of the MODIS sensor, which is orbiting the Earth on board two satellites, Terra and Aqua. We have chosen MODIS because of its daily revisit time combined with a spatial resolution of 500 m, which is higher than our ICAR simulation. More specifically, we have used the Normalized Difference Snow Index (NDSI) retrievals of collection 6 of the NASA snow-cover products MOD10A1 (Terra) (Hall et al., 2006) and MYD10A1 (Aqua) (Hall and Riggs, 2016) distributed by the National Snow and Ice Data Center. To estimate the fSCA from the MODIS NDSI we

210 have used a linear function following Salomonson and Appel (2004). The coefficients of
the function were optimized using a serie of 20 m resolution snow products from Theia
Snow collection (Gascoin et al., 2019). The Theia Snow collection provides snow cover
area maps derived from Sentinel-2 observations. The revisit period of Sentinel-2 is at
most 5 days since the launch of Sentinel-2B (i.e. after march 2017). It can be shorter in
215 areas where successive swaths overlap laterally. We downloaded 645 Theia Sentinel-2
snow products acquired between 2017-09-03 and 2018-12-24 over Lebanon. For every
Sentinel-2 image we can match a MODIS image since there is a MODIS image every day
over Lebanon during the same period. Theia binary snow maps were resampled to 500 m
fSCA in the same grid as the MODIS products by averaging the contributing pixels. By
220 comparing these fSCA Theia maps with the MOD10A1 products we could find 5.84×10^4
cloud-free pixels which corresponded to MOD10A1 snow-covered pixels on the same
date. A subset of 40% of the NDSI-fSCA were used to fit the linear function using the
least squares method. The optimized function was tested against the remaining data and
yielded an fSCA RMSE of 11% and a mean absolute error of 5.7%. The same analysis
225 was done with MYD10A1 (Aqua) products but we opted not to use them in the
remainder of the analysis because they exhibited a lower agreement with the Theia
Sentinel-2 snow cover products (RMSE of 21%). The lower agreement of MYD10A1 is
likely due to degraded sensors (Wang et al., 2012) but may also be related to the
difference between the overpass time of Sentinel-2 (10:30 local time) and Aqua (13:30
local time), while Terra share the same overpass time as Sentinel-2.

230 We reprojected the generated MODIS fSCA products to the spheroid datum (6370 km
earth radius) Lambert conformal projection used in the ICAR simulation. To avoid
artifacts as consequence of the data gaps of MODIS imagery caused by the cloud cover,
we have performed the aggregation when the majority of the MODIS cells used to
calculate each new resampled cell was cloud free (less than 25% cloud cover), otherwise
235 the cell was considered empty missing for the scene in question. In previous studies, the
MODIS fSCA products have shown to have a good performance retrieving fSCA
information compared with field observations even considering its moderate resolution
(Aalstad et al., 2020). Thus, they are a robust resource to use when developing regional
scale snow reanalysis.

240 3.2.2 Particle batch smoother implementation

The assimilation procedure was implemented using the PBS scheme (Margulis et al.,
2015). The PBS assigns a weight to each ensemble member according to its agreement
with the observations through Bayes theorem. The most obvious advantage of this
technique is its computational efficiency, as it avoids the resampling step common in
245 other assimilation algorithms. A complete description of the PBS can be found in
Margulis et al. (2015). It is also summarized in Aalstad et al. (2018) and Fiddes et al.
(2019). The PBS has been shown to perform well relative to other assimilation algorithms
when used to assimilate fSCA information (Aalstad et al., 2018; Margulis et al., 2015),
even though it can suffer from particle degeneracy as consequence of a highly
250 inhomogeneous distribution of weights (Van Leeuwen, 2009). In this context, the PBS

has been successfully used to develop a series of snowpack reanalyses (Cortés et al., 2016; Fiddes et al., 2019; Margulis et al., 2016).

255 For the prior of the PBS implementation, we generated an ensemble of snowpack simulations forcing the FSM2 (Essery, 2015), with the ICAR predicted surface meteorology. The configuration of the FSM2 model includes an albedo correction as snow ages with time differently for melting and cold snow, and increases with snowfall with a maximum of 0.9. The compaction rate was calculated based on overburden and thermal metamorphism (Verseghy, 1991). The turbulent exchange coefficient was stability corrected based on the bulk Richardson number. The thermal conductivity was
260 calculated based on snow density. Finally, the FSM2 configuration accounted for retention and refreezing of water inside the snowpack. Such a configuration has been shown to properly simulate the inter- and intra-annual variability of the snowpack dynamics over mountains with a similar Mediterranean climate (Alonso-González et al., 2018).

265 To generate the ensemble of forcing datasets, we perturbed the precipitation and the 2 m air temperature surface fields of the ICAR output using a log-normal and a normal (Gaussian) probability density functions respectively. We choose the mean of the probability functions from the averaged biases of the ICAR simulation, estimated from independent observations provided by three mountain AWS at the locations shown in
270 Figure 1 (Fayad et al., 2017a). The variance of the probability distribution functions was calculated by doubling the variance of the errors to increase the spread of the ensemble to cover the apparent uncertainty in the ICAR outputs. The precipitation phase had to be recalculated for the new synthetic temperatures for each ensemble member. Due to the strong dependency of the snowpack over Lebanon on precipitation phase, a simple
275 temperature threshold based precipitation phase partitions are not recommended (Fayad and Gascoin, 2020). Instead, we have used the psychrometric energy balance method approach proposed by Harder and Pomeroy (2013), where the precipitation phase is estimated by means of the estimation of the temperature of the falling hydrometeor calculated from the air temperature and relative humidity. A total of 400 ensemble
280 members per ICAR cell were independently generated by randomly drawing multiplicative time-constant parameters from the log-normal probability function for precipitation, and additive parameters from the normal probability function for the 2 m air temperature.

To estimate the fSCA of each ensemble member we used the probabilistic snow depletion
285 curve proposed by Liston (2004). This model simulates the subgrid peak SWE distribution using a lognormal probability density function. Then, the fSCA is diagnosed using the accumulated melt depth estimated from the energy balance outputs of the FSM2, the peak mean SWE, and the peak subgrid coefficient of variation (CV) of the lognormal probability density function, assuming a constant melt over the grid cell. The
290 CV used in this model is strongly controlled by the characteristics of the terrain. We have included the CV parameter as part of the assimilation, perturbing its value inside the recommended values in Liston (2004) using a mean of 0.4 and a variance of 0.01

295 (Aalstad et al., 2018). The PBS was implemented over the fSCA ensemble over each grid cell and season independently, using the values of the melting season, corresponding to the months of March through June. Finally, the generated SWE products (ICAR_assim hereafter) were estimated from the weighted mean of the SWE of the ensemble members, where the weights were obtained using the PBS. A schematic description of the whole process is presented in Figure 2.

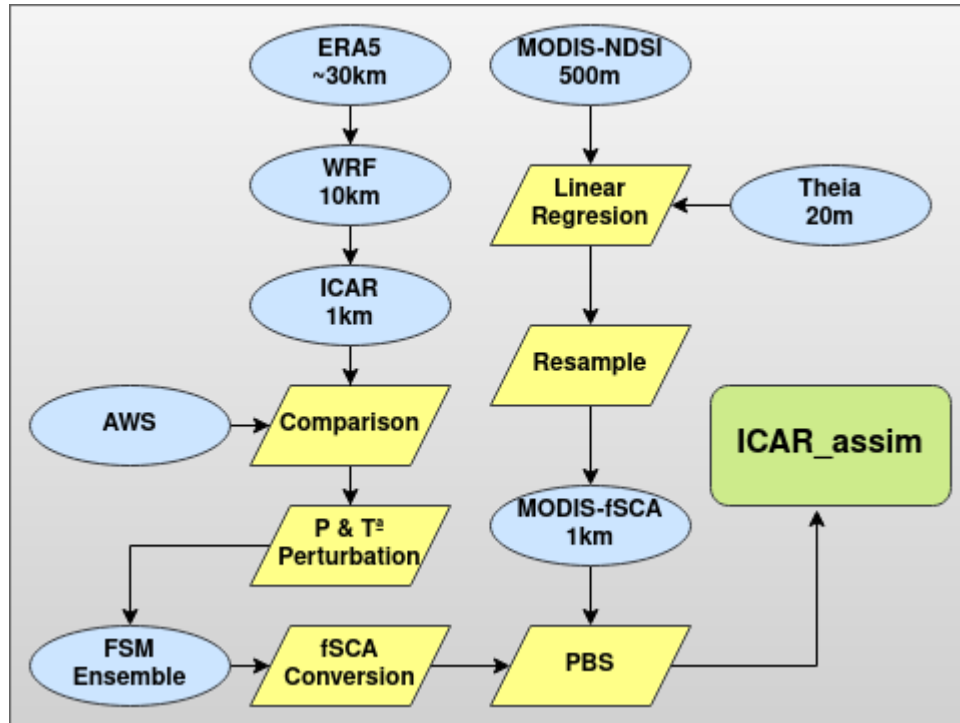


Figure 2: Schematic flow chart of the ICAR_assim snow product development

300 3.3 Validation procedure and analysis of the SWE products

305 The ICAR atmospheric simulation and the ICAR_assim products were compared against independent observations. First, the ICAR atmospheric simulation was compared with three AWS located in the main mountain range of the domain (Fayad et al., 2017a)(Figure 1). Temperature and precipitation measurements were aggregated to the hourly model output frequency from the original 30-minute time resolution. Then, the temperature and precipitation biases were estimated. The precipitation data was available only in two of the AWS. The error values and its variance were used to define the shape of the probability density functions of the perturbation parameters described above to generate each ensemble.

310 *Table 1: AWS geographical coordinates and elevations. Elevation of the ICAR cell that contains each AWS.*

AWS	Snow seasons	Elevation [m a.s.l.]	Latitude (WGS84)	Longitude (WGS84)	ICAR elevation [m a.s.l.]
A	2013 to 2016	2834	34.27° N	36.09° E	2827
B	2014 to 2016	1843	34.14° N	35.88° E	1746
C	2011 to 2016	2296	33.98° N	35.86° E	2272

315 After the PBS implementation, we compared the ICAR and ICAR_assim snow products with the snow depth observed information derived from a Campbell SR50A acoustic gauge at the three AWS. The observed snow depth was transformed into SWE by
 320 assuming a constant snow density value of 467 kg m^{-3} , estimated from observations in the area (Fayad et al., 2017a). That was necessary to make the AWS data comparable with the ICAR snow outputs as they are provided only as SWE. Even if it is commonly implemented in operational atmospheric forecast models, the assumption of a constant density could introduce obvious bias in the SWE estimation (Dawson et al., 2017). In the
 325 Mediterranean snowpacks, such biases are partially reduced as consequence of the high densification rates of the snowpack (Bormann et al., 2013; Fayad et al., 2017b). However, we introduced a sensitivity analysis in the comparison, varying the density value in the range of $\pm 15\%$ to illustrate such uncertainty. To compensate the big shift between the ICAR and ICAR_assim resolutions (1 km x 1 km) and the point-scale nature of the AWS observations, we have interpolated a new SWE series from the 4 nearest cells of the simulations using the inverse distance method.

330 The spatial accuracy of the SWE products was compared to satellite observations. First, we developed a daily gapfilled snow cover time series covering the time period of the ICAR simulation from the MODIS snow cover products using the methodology proposed by Gascoin et al. (2015). Then, the products were aggregated to estimate the averaged snow presence over each cell in percentage ($P(\text{snow})$). The MODIS $P(\text{snow})$ product was aggregated to the ICAR grid to make it comparable. Then, we calculate the $P(\text{snow})$ for the ICAR and ICAR_assim simulations. We choose a SWE MODIS detection threshold of 20 mm to calculate the $P(\text{snow})$ from the simulated SWE series, inside the
 335 range recommended by Gascoin et al. (2015). All the spatial analysis and the data assimilation was computed over the areas that had exhibited a $P(\text{snow}) > 5\%$, which amounts to a total surface of 4412 km^2 .

4. Results and Discussion

4.1 Atmospheric simulation results

340 The use of ICAR is justified as it is computationally inexpensive compared to similar
WRF simulations, while retaining a physical basis to enable simulations in regions
lacking observations. The speed up factors can range from 140 in its more complex
configurations (as choose for this study) to 800 in its simpler configurations (Gutmann et
al., 2016). However, the linear theory simplification presents some limitations when
345 predicting the motion of the atmosphere, such as interactions between waves and
turbulence (Nappo, 2012) or the lack of explicit convection. Despite these limitations,
ICAR has been shown to be a valuable tool for downscaling showing a good consistency
with observations (Horak et al., 2019), as well as with fully dynamical WRF simulations
(Gutmann et al., 2016). Figure 3 shows how the ICAR model was able to improve the 2
350 m air temperature data, compared with the ERA5 reanalysis (ICAR mean error= 2.8°C
compared with 8.5°C in ERA5), showing comparable performances with the WRF
coarser simulation (WRF mean error = 2.3 °C). It was not expected to improve the parent
WRF simulation with ICAR, but the increase of resolution was necessary as the
snowpack simulations requires higher resolutions. The coarser ERA5 resolution that
355 smooths the terrain leads to warm biases. This is particularly evident in the Lebanon
ranges where the elevation gradient ranges from 0 to 3000 m a.s.l. in approximately 25 km
(Figure 1). Despite the clear improvement in the temperature performance, the simulation
is biased towards slightly higher temperatures than the AWS data. However, the main
temporal patterns and the magnitude of the temperature are well represented.

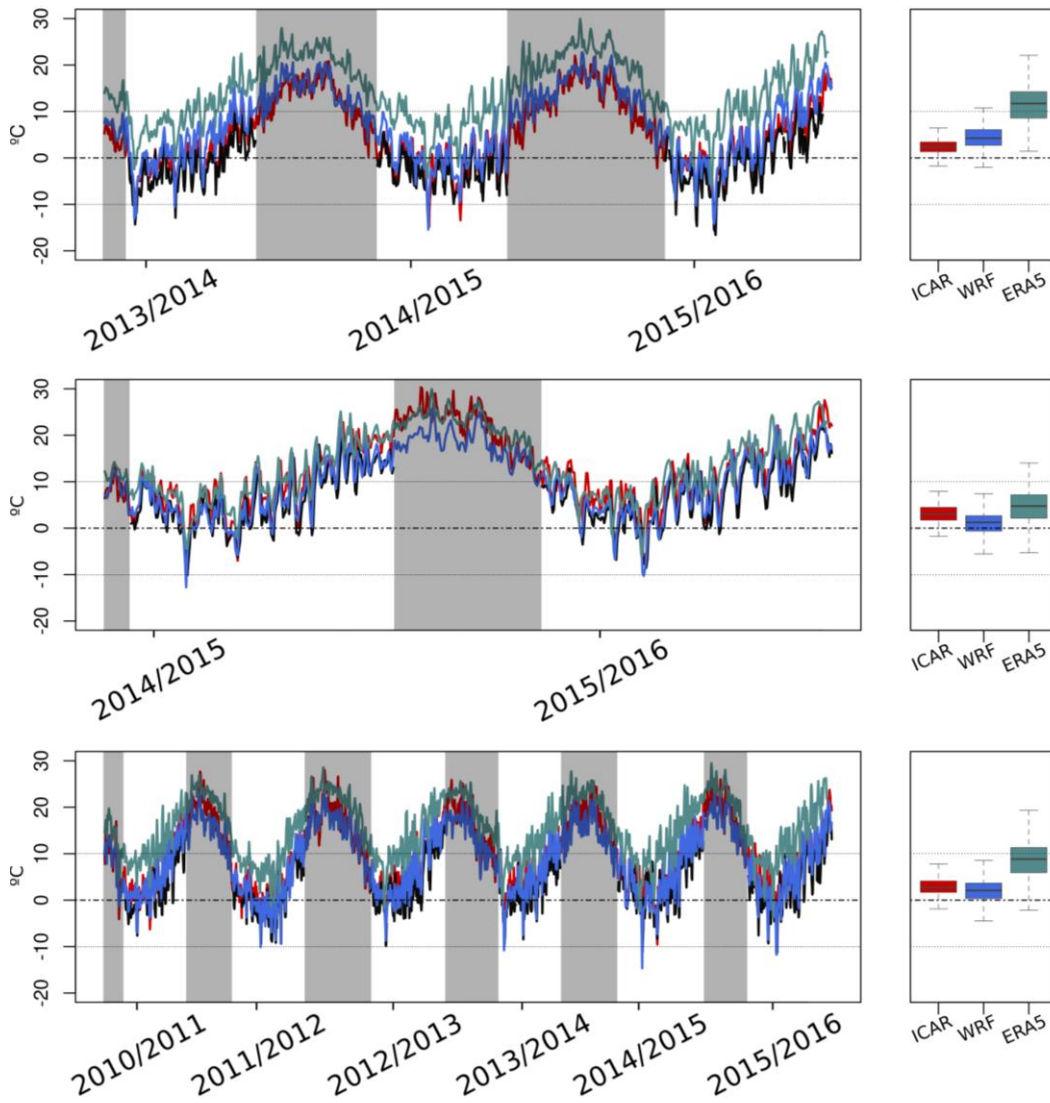


Figure 3: ERA5 (green), WRF (blue), ICAR (red) and AWS (black) daily temperature data. The boxplots represent the distribution of the errors and the gray shadows the data gaps in the observations.

360

Similarly, precipitation outputs of ICAR were compared with the gauges deployed in two of the AWS sites. ICAR reduces the spread of the daily precipitation errors of ERA5 as shown in Figure 4 (standard deviation of 11.5mm in ERA5 compared with the 8.4mm of ICAR), even though the ERA5 error are already surprisingly low considering the spatial resolution and the fact that precipitation is challenging to simulate by numerical models especially over complex terrain (Legates, 2014). This validation provides a range of uncertainty estimates to help generate the probability density functions for the perturbations of the ensemble. The selected parameters to define the shape of the normal

365

probability density function which defines the additive perturbation to the temperature were set to a mean of $-3.0\text{ }^{\circ}\text{C}$ and a variance of $1.8\text{ }^{\circ}\text{C}$. Similarly, the parameters of the lognormal probability density function used to obtain the multiplicative perturbation factors for the precipitation were a mean of 2.0 and a variance of 0.75. Even though the parameters were designed to model the uncertainty of ICAR, they are similar to comparable implementations of the PBS (Cortés et al., 2016). Through the forced increase of the variance of the probability density functions, we ensure that the ensemble of snow simulations covers the expected uncertainty space of ICAR, while the PBS has proved to be robust to progressive variations of the perturbation parameters (Cortés et al., 2016).

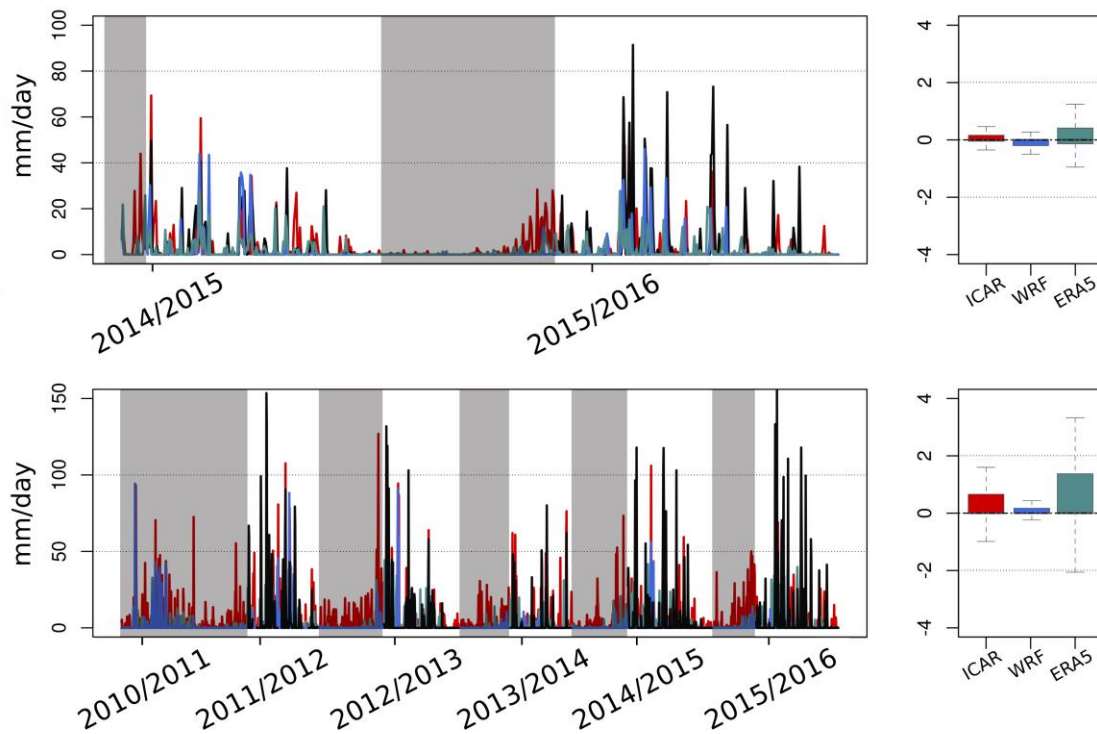


Figure 4: ERA5 (green), WRF (blue), ICAR (red) and AWS (black) daily precipitation data. The boxplots represent the distribution of the errors and the gray shadows the data gaps in the observations.

380 4.2 Fractional snow cover assimilation

The new proposed linear relationship function to derive fSCA from NDSI has improved the MODIS fSCA products when compared with the relationship function by Salomonson and Appel (2004) (Supplementary figure 1). Using the relationship function by Salomonson and Appel (2004) resulted in larger mean absolute error (MAE) (6.2% com-

385 pared to 5.7%) and Root Mean Squared Error (RMSE) (12% compared to 11%). The
equation of the linear fit is:

$$fSCA = 1.23 \cdot NDSI + 0.23$$

The performance of ICAR_assim was compared against snow depth measurements at the
AWS locations (Figure 5) and MODIS gapfilled products (Figures 6 and 7). In general,
390 ICAR has a tendency to underestimate the SWE compared with ICAR_assim. This is
likely related to the warm biases detected in the simulation, combined with the limitations
of the snow model implemented in the Noah land surface model used by ICAR (Barlage
et al., 2010). Thus, future versions of ICAR with better representations of the snow
processes through the implementation of more complex land surface parametrizations
395 like Noah-MP (Niu et al., 2011), as used in the parent WRF simulation, could potentially
improve the accuracy of ICAR's SWE outputs (Suzuki and Zupanski, 2018). This effect
could be particularly enhanced in the mild climatic conditions of Lebanon, as larger
disagreements in the SWE outputs between Noah and Noah-MP occur under warm
conditions (Kuribayashi et al., 2013). However, the improvement of the snow
400 representations of ICAR is clear when compared with ERA5 reanalysis which was not
able to reproduce the snowpack at all due to its coarse resolution.

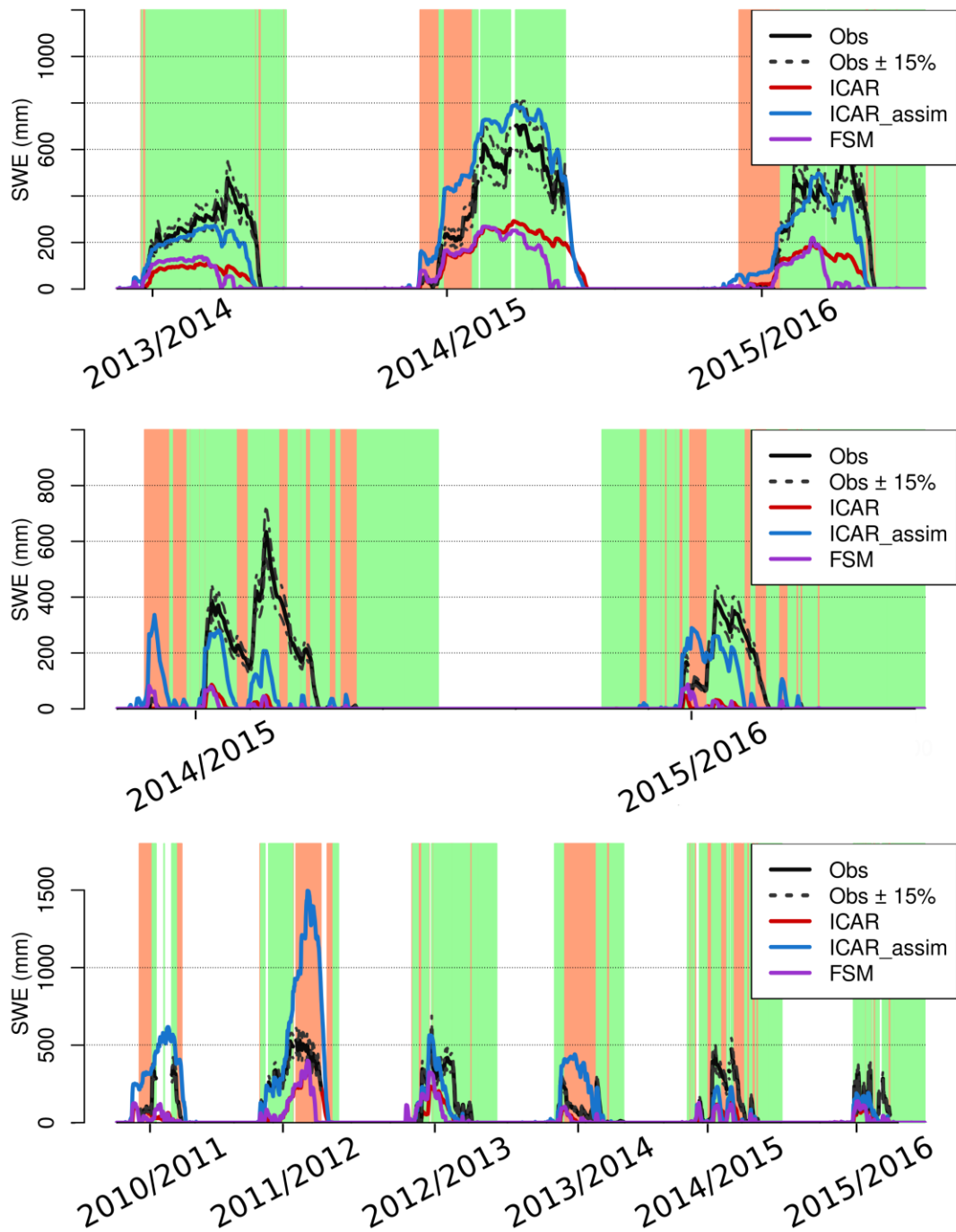


Figure 5: Comparison between observed, ICAR, FSM, and ICAR_assim. SWE products. The green in the background indicates the time steps when ICAR_assim improves the performance of ICAR.

405 The use of FSM to generate the ensemble of simulations, introduced some uncertainties
in the workflow. Some water years showed earlier snow melts using the FSM forced by
ICAR, compared with the ICAR snow outputs. As the uncertainty of the snow models
associated to the forcing is higher than the uncertainty associated by the use of different
410 model parameterizations and model structures (Günther et al., 2019), we hypothesize that
such differences were caused by the differences in the precipitation phase partitioning,
which is challenging to simulate in the areas that remain close to 0 °C during the snow
season (Fayad and Gascoin, 2020). The lack of spring snowfalls in some years may have
deep implications in the snowpack simulation that are not limited to its effect in the mass
balance and the releasing of latent heat by refreezing the liquid precipitation. It leads to
415 lower albedos, which combined with the high short-wave radiation of Lebanon due to its
latitude causes earlier snow melts. However, such discrepancies are greatly minimized in
ICAR_assim, by the assimilation of the fSCA retrievals

The results of the validation of ICAR_assim show a good agreement with the
observations. For the estimated SWE, the RMSE and the MAE relative to the AWS were
420 189.2 mm and 104.52 mm respectively after removing the summer from the analyses,
with a coefficient of correlation (R) of 0.75 for the annual mean SWE accumulation. Even
though ICAR_assim generally shows a good agreement with the observations (especially
considering the scale mismatch between the stations and ICAR_assim), some clear
differences were found. Figure 5 exhibits a surprisingly high difference in the magnitude
425 of the observed SWE and the ICAR_assim output for the 2011/2012 winter season in the
third AWS. However, independent observations in the area have described an exceptional
snowpack in this season, with snow depths more than 6 m even reaching up to 10 m
locally (Koeniger et al., 2017). Such disagreements between the AWS information and
the independent observations can be explained by the high spatial heterogeneity of the
430 snow depth at point scales (López-Moreno et al., 2011). This effect was studied in the
Atlas mountains, where the agreement of the snow simulations rapidly drops using
resolutions over 250 m (Baba et al., 2019). Such spatial heterogeneity has been shown to
be particularly high over mount Lebanon due to the important role of the wind
redistribution as consequence of geomorphology (Fayad and Gascoin, 2020). For
435 example, Fayad and Gascoin (2020), reported large differences with the AWS data from
in situ measurements on 15 of January 2016, when they measured snow depths up to 258
cm on the surroundings of the third AWS location (Figure 5; bottom panel), while the
AWS sensor itself detected 7.5 cm. However, the comparison between the temporal
patterns of the snow cover over Lebanon from MODIS gap-filled daily products and
440 ICAR_assim have shown good levels of agreement with a RMSE=270.2 km², a
MAE=124.1 km² over a total surface of 4412km² (Figure 6), and a Pearson correlation
value of R=0.88 in the annual maximum of the snow cover extent (Figure 6). The larger
spatial support of the MODIS products permits a more representative and extensive
validation of ICAR_assim. Thus, the good agreement between both snow cover products

445 and the generally SWE magnitudes with the AWS observations shows the temporal consistency of the ICAR_assim reanalysis.

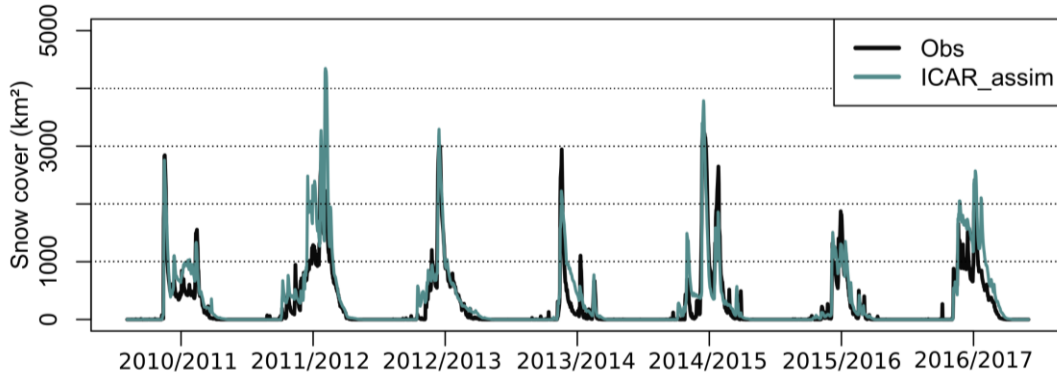


Figure 6: Daily snow cover extent comparison between MODIS gapfilled products and ICAR_assim.

The spatial patterns of ICAR_assim, were also compared with the MODIS gapfilled products (Figure 7). The spatial comparison of the $P(\text{snow})$ showed a very good level of agreement demonstrating the potential of fSCA assimilation through the PBS in improving the ICAR SWE products. The comparison showed a correlation value of $R=0.98$, a RMSE=3.0 % and a MAE=2.3 % improving the ICAR simulation that exhibited values of $R=0.79$, RMSE=14.3% and MAE=12.3%. There was a general tendency to slightly underestimate the $P(\text{snow})$ values by ICAR_assim, specially at the lower elevations. We hypothesize that this effect could be caused by the selection of a constant SWE depth to calculate the snow cover from the ICAR_assim product. Thus, the shallow snowpacks whose SWE values are under the selected threshold are not recorded as snow presence in the ICAR_assim even though they could potentially be detected as snow by the MODIS sensor. In addition, the MODIS snow cover products should be considered less accurate over areas of rapid melt (Gascoin et al., 2015). Such mismatch between ICAR_assim and MODIS combined with the fact that the 2011 – 2012 snow season showed persistent cloud covers related with its exceptional snowpack, could explain the biases in the Figure 6. During the 2011 – 2012 snow season, the gapfilling algorithm had less information to fill the MODIS snow cover time series, while the PBS had propagated the fSCA information through the whole season from the few available observations. In summary, our results have shown how ICAR_assim can accurately reproduce the inter-annual and intr-annual spatiotemporal patterns of the snow cover, with a SWE magnitude comparable with independent observations that agree well in terms of temporal patterns.

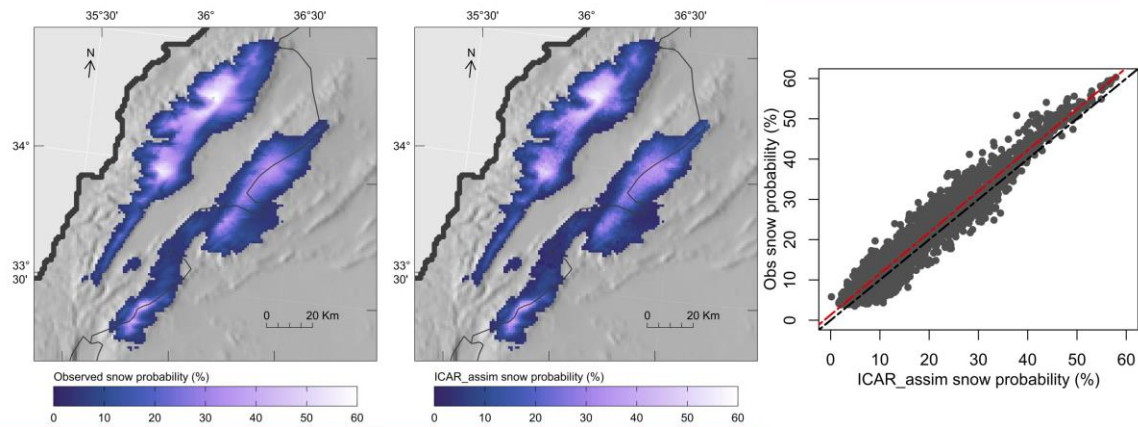


Figure 7: Snow probability spatial comparison between observed MODIS products and ICAR_assim.

470 4.3 Snowpack dynamics over Lebanon mountains

ICAR_assim exhibits some limitations that should be considered. First, despite the high resolution of the reanalysis the regional nature of the simulations prevent the representation of some processes like wind or avalanches snow redistribution. In addition, there are some other sources of uncertainty involved in the development of the reanalysis, like the depletion curve, the fSCA derived from MODIS or the structural uncertainty associated with each model. However, ICAR_assim has been shown to be consistent with the limited observations providing a valuable resource in the data scarce context of the Lebanese mountains.

Figure 8 shows the spatial distribution of the mean peak SWE values and its temporal coefficient of variation for the 2010-2017 time period. Such values can be influenced by the fact that the study period is relatively humid compared with the previous years (Cook et al., 2016), showing slightly higher values than a long term climatology. However, the length of the reanalyses constitutes a reasonably representative sample of the main snowpack dynamics over the region. The snowpack over Lebanon has exhibited the high temporal variability that is characteristic of the Mediterranean snowpacks (Fayad et al., 2017b), with similar values of the coefficient of variation as those observed in other Mediterranean mountain ranges (Alonso-González et al., 2020). The maximum accumulations reach 2000 mm of SWE and are located at the higher elevations of mount Lebanon, where there is a plateau over the elevation of the winter zero isotherm (Fayad and Gascoin, 2020). The temporal coefficient of variation of the annual peak SWE follows unequal spatial patterns, . It tends to exhibit higher values over the areas sheltered from direct interaction with the warm and moist Mediterranean air. In addition it exhibits a decreasing trend with elevation (Figure 9) as found in other Mediterranean ranges (Alonso-González et al., 2020), reaching a minimum of 15%.

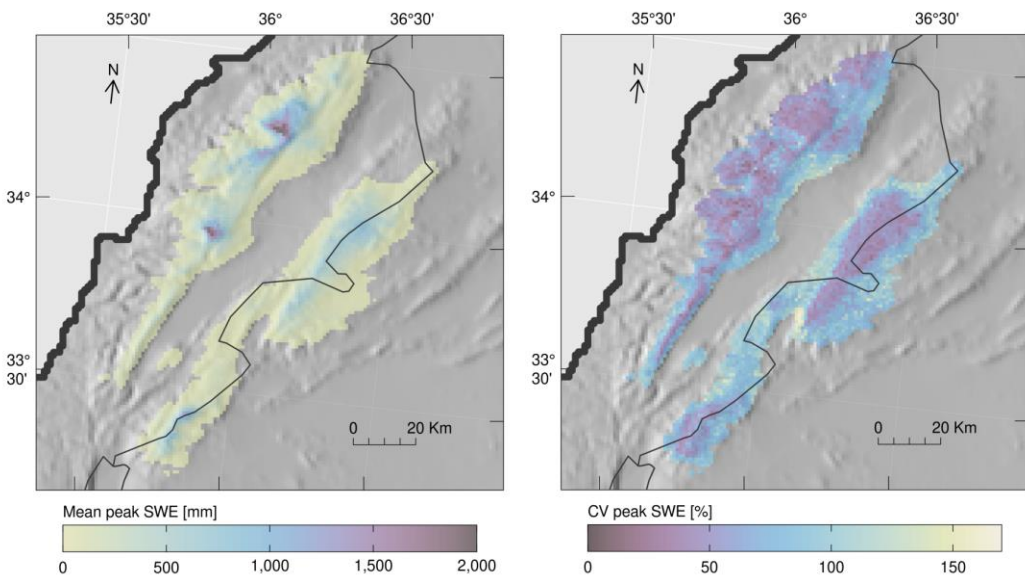


Figure 8: Averaged annual peak SWE (left) and annual coefficient of variation (right).

There are clear differences between the Lebanon and Anti-Lebanon ranges, that can be just partially explained by their different orography. Despite the closeness of both Lebanon and Anti-Lebanon ranges, they exhibit different relationships between the values of mean peak SWE (Figure 9 top panel) and snow duration (Figure 9 bottom panel) and with the elevation, showing that the differences are not just related to the particular orography of each range, but also with its climatological characteristics. Thus, at comparable elevations mount Lebanon tends to show higher values of $P(\text{snow})$ and mean peak SWE, with lower values of coefficient of variation, suggesting thicker, longer lasting and seasonally stable snowpack. The orographic precipitation caused by the uplift of the Mediterranean moisture is a major source of precipitation in the area (Jomaa et al., 2019) That is probably why Anti-Lebanon mountains shows lower peak accumulations than Mount Lebanon, with Anti-lebanon in the rain shadow leading to lower precipitation and snow accumulation. However, despite the differences in the coefficient of variation values, they tend to become similar at the higher elevations. The same coefficient of variation occurs in the elevations where the precipitation leads the snow accumulation while they differ at the lower elevations, where the accumulation is conditioned by the temperature. This effect suggest warmer conditions on the Anti-Lebanon mountain as consequence of leeside wind effects (Foëhn type effect), and confirm the sensitivity of the snow simulation to the chosen partition phase method over Mediterranean mountains (Fayad and Gascoin, 2020).

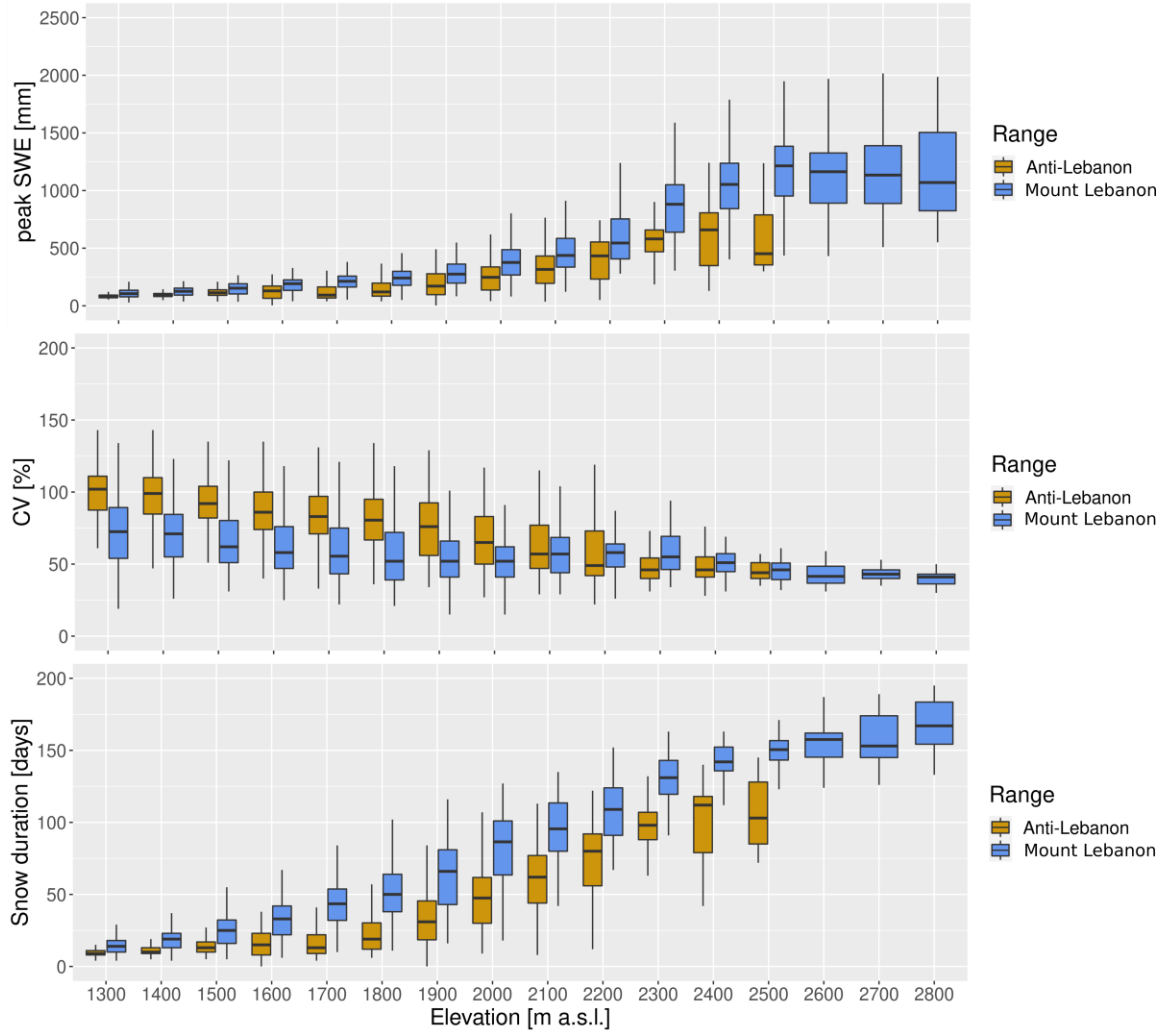


Figure 9: Relationship between annual peak SWE and elevation (top), coefficient of variation and elevation (middle), and snow duration and elevation (bottom).

Figure 10 shows the averaged seasonal SWE accumulation at different elevations over both the Lebanon and Anti-Lebanon ranges. Each elevation represents the aggregated pixels of the elevation with a range of ± 50 m a.s.l. For reference, they show on average a peak SWE of 306 mm at the elevation band of 2000 m a.s.l., which is comparable to those found in the Iberian Peninsula mountain ranges (Alonso-González et al., 2020). More specifically, the peak SWE and duration values shows intermediate values between the Central Iberian and Pyrenees ranges at 2000 m a.s.l, but with a peak SWE coefficient of variation of 53 %, that is greater than the highest values of Iberia located at Sierra Nevada with 34 %. The relative area lying at each elevation compared with the total elevation over 1300 m a.s.l. is represented to highlight the importance of the hypsography from the hydrological point of view. Thus, Lebanon exhibits a deep and long lasting snowpack with up to 1000 mm of peak SWE on average particularly over 2500 m a.s.l.,

but the relative areal coverage of such elevations is very low. This suggest that the mean peak SWE series at lower elevations could hide a large variation in mass due to the wider areas at lower elevations where many different peak SWE values can coexist, as Alonso-González et al.(2020) found in the Iberian mountain ranges.

535

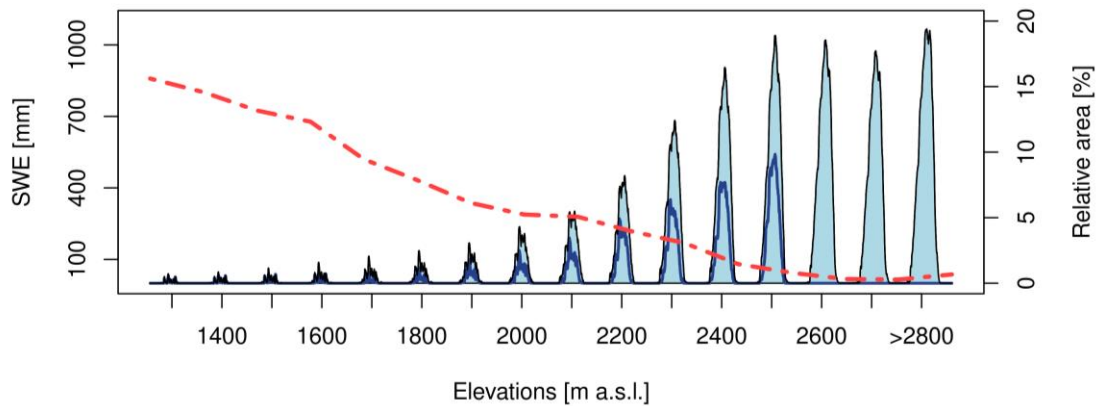


Figure 10: Mean annual evolution of SWE at different elevation bands. Dark blue line represent the Anti-lebanon range, black line the Mount Lebanon range, and red line the relative areal coverage of each elevation above 1300 m a.s.l.

The thick snowpacks found at the higher elevations are not necessarily the biggest fresh water resources available due to the hypsometry of the mountain area. Figure 11 shows the average amount of freshwater stored in the snowpack per elevations band. It is obvious that the maximum amount of freshwater is stored between 2100 to 2500 m.a.s.l., despite the fact that thicker snowpacks are at higher elevations. The cumulative water storage in the snowpack is more than double in the medium elevation zone (average maximum up to 552 Hm³ from 1300 to 2300m a.s.l.) when compared to the higher areas (average maximum up to 189 Hm³ at 2400 m a.s.l. and onward). This is an important part of the yearly water budget, as mean annual precipitation was estimated in to be 7200 Hm³ for the period (2010-2016) (Jaafar et al., 2020). Noting that this in contrast to the fact that the orography of Lebanon encourages the storage of snow in the upper areas because of the existence of a high elevation plateau(Fayad et al., 2017a; Fayad and Gascoïn, 2020). These results suggest new challenges for the water management of Lebanon in the future as a consequence of warming climate. The snowpack at low elevation areas is more sensitive to warming (Jefferson, 2011; Marty et al., 2017; Sproles et al., 2013), particularly over areas with mild winter conditions as has been shown in other Mediterranean regions (Alonso-González et al., 2020a).

540

545

550

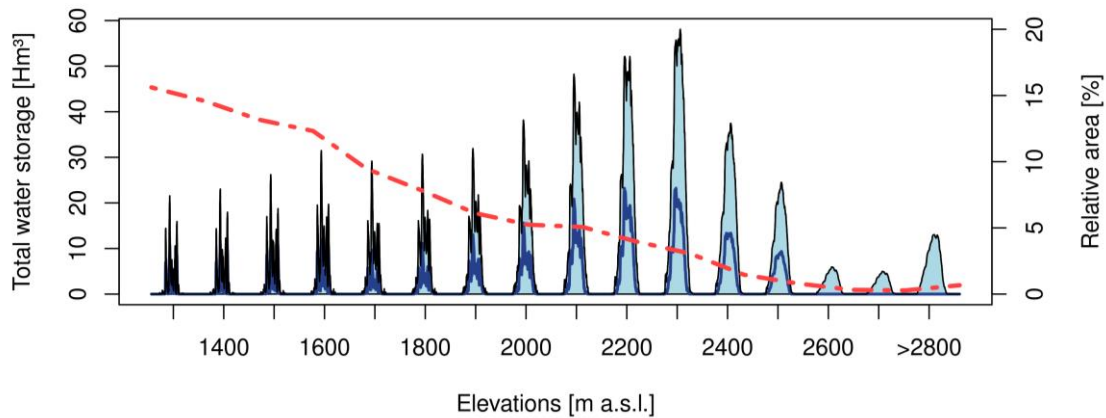


Figure 11: Averaged annual water stored in the snowpack at different elevation bands. Dark blue line represent the Anti-Lebanon range, black line the Mount Lebanon range, and red line the relative areal coverage of each elevation above 1300 m a.s.l.

555 5. Conclusions

The assimilation of MODIS fSCA through the use of the PBS has proven to be a cost effective way to use remote sensing data in snow simulations, and is particularly appropriate for simulating snow in data scarce regions. Thus, the generated SWE products show good agreement with MODIS snow cover gapfilled data, with $R = 0.98$, $RMSE = 3.0 \%$ and $MAE = 2.3 \%$ for the spatial map of the probability of snow. The time series of snow cover showed a $R=0.88$, $RMSE=270.2 \text{ km}^2$, and $MAE=124.1 \text{ km}^2$ over a total surface of 4412 km^2 . The performances in terms of SWE magnitude with the few available point-scale observations was $R=0.75$, $RMSE=189.2 \text{ mm}$, and $MAE = 104.5 \text{ mm}$ after removing the summer from the analyses.

565 The snowpack over Lebanon is characterized by a high temporal variability. Some differences exist between its two main mountain ranges. Mount Lebanon exhibits thicker, longer and more regular snowpacks compared to the Anti-Lebanon range. Such differences cannot only be explained by the elevation difference but also reflects the dryer conditions on the leeward side of the Mount Lebanon range due to the rain shadow effect.

570 The hypsometry of Lebanon results in the most important snow freshwater reservoir being in the middle elevations (2200-2500 m a.s.l.). Snowpacks at these elevations close to the $0 \text{ }^\circ\text{C}$ isotherm are highly vulnerable to climate warming. As such, our findings suggest big challenges for the future management of water resources over the Lebanon region.

575

Acknowledgments: Esteban Alonso-González is supported by the Spanish Ministry of Economy and Competitiveness (BES-2015-071466). This study was funded by the Spanish Ministry of Economy and Competitiveness projects CGL2014-52599-P10 (IBERNIEVE) and CGL2017-82216-R (HIDROIBERNIEVE). We acknowledge support
580 of the publication fee by the CSIC Open Access Publication Support Initiative through its Unit of Information Resources for Research (URICI). Kristoffer Aalstad was funded by the Satperm project (239918; Research Council of Norway), a Personal Overseas Research Grant (Research Council of Norway), and the European Space Agency Permafrost CCI project (<http://cci.esa.int/Permafrost>), and acknowledges support from
585 the LATICE strategic research area at the University of Oslo.

Code and data availability: WRF code can be downloaded from <https://www2.mmm.ucar.edu/wrf/users/downloads.html>. ICAR code can be found at <https://github.com/NCAR/icar>. FSM2 is archived at <https://github.com/RichardEssery/FSM2>. The meteorological data can be found at
590 <https://doi.org/10.5281/zenodo.583733>.

Author Contribution: EAG: Conceptualization, Methodology, Writing – original draft, Software, Data curation, Validation, Visualization. EG: Methodology, Software, Supervision, Writing – review & editing. KA: Conceptualization, Methodology, Software, Writing – review & editing. AF: Methodology, Conceptualization, Writing –
595 review & editing. MB: Data curation, Software, Writing – review SG: Conceptualization, Data curation, Methodology, Supervision, Writing – review & editing.

Conflicts of Interest: The authors declare no conflict of interest in this article

References

- 600 Aalstad, K., Westermann, S., Bertino, L., 2020. Evaluating satellite retrieved fractional snow-covered area at a high-Arctic site using terrestrial photography. *Remote Sens. Environ.* 239, 111618. <https://doi.org/10.1016/j.rse.2019.111618>
- Aalstad, K., Westermann, S., Schuler, T.V., Boike, J., Bertino, L., 2018. Ensemble-based
605 assimilation of fractional snow-covered area satellite retrievals to estimate the snow distribution at Arctic sites. *Cryosphere* 12, 247–270. <https://doi.org/10.5194/tc-12-247-2018>
- Albergel, C., Dutra, E., Munier, S., Calvet, J.C., Munoz-Sabater, J., De Rosnay, P., Balsamo, G., 2018. ERA-5 and ERA-Interim driven ISBA land surface model simulations: Which one performs better? *Hydrol. Earth Syst. Sci.* 22, 3515–3532.
610 <https://doi.org/10.5194/hess-22-3515-2018>

- Alonso-González, E., Ignacio López-Moreno, J., Gascoin, S., García-Valdecasas Ojeda, M., Sanmiguel-Vallelado, A., Navarro-Serrano, F., Revuelto, J., Ceballos, A., Esteban-Parra, M.J., Essery, R., 2018. Daily gridded datasets of snow depth and snow water equivalent for the Iberian Peninsula from 1980 to 2014. *Earth Syst. Sci. Data* 10, 303–315. <https://doi.org/10.5194/essd-10-303-2018>
615
- Alonso-González, E., López-Moreno, J.I., Navarro-Serrano, F., Sanmiguel-Vallelado, A., Aznárez-Balta, M., Revuelto, J., Ceballos, A., 2020. Snowpack sensitivity to temperature, precipitation, and solar radiation variability over an elevational gradient in the Iberian mountains. *Atmos. Res.* 243, 104973.
620 <https://doi.org/10.1016/j.atmosres.2020.104973>
- Alonso-González, Esteban, López-Moreno, J.I., Navarro-Serrano, F., Sanmiguel-Vallelado, A., Revuelto, J., Domínguez-Castro, F., Ceballos, A., 2020. Snow climatology for the mountains in the Iberian Peninsula using satellite imagery and simulations with dynamically downscaled reanalysis data. *Int. J. Climatol.* 40, 477–491.
625 <https://doi.org/10.1002/joc.6223>
- Arasa, R., Porrás, I., Domingo-Dalmau, A., Picanyol, M., Codina, B., González, M.Á., Piñón, J., 2016. Defining a Standard Methodology to Obtain Optimum WRF Configuration for Operational Forecast: Application over the Port of Huelva (Southern Spain). *Atmos. Clim. Sci.* 06, 329–350. <https://doi.org/10.4236/acs.2016.62028>
- 630 Baba, M.W., Gascoin, S., Hanich, L., 2018a. Assimilation of Sentinel-2 data into a snowpack model in the High Atlas of Morocco. *Remote Sens.* 10, 1982.
<https://doi.org/10.3390/rs10121982>
- Baba, M.W., Gascoin, S., Jarlan, L., Simonneaux, V., Hanich, L., 2018b. Variations of the snow water equivalent in the ourika catchment (Morocco) over 2000-2018 using
635 downscaled MERRA-2 data. *Water (Switzerland)* 10, 1120.
<https://doi.org/10.3390/w10091120>
- Baba, M.W., Gascoin, S., Kinnard, C., Marchane, A., Hanich, L., 2019. Effect of Digital Elevation Model Resolution on the Simulation of the Snow Cover Evolution in the High Atlas. *Water Resour. Res.* 55, 5360–5378.
640 <https://doi.org/10.1029/2018WR023789>
- Bakalowicz, M., El Hakim, M., El-Hajj, A., 2008. Karst groundwater resources in the countries of eastern Mediterranean: The example of Lebanon. *Environ. Geol.* 54, 597–604. <https://doi.org/10.1007/s00254-007-0854-z>

- 645 Barlage, M., Chen, F., Tewari, M., Ikeda, K., Gochis, D., Dudhia, J., Rasmussen, R.,
Livneh, B., Ek, M., Mitchell, K., 2010. Noah land surface model modifications to
improve snowpack prediction in the Colorado Rocky Mountains. *J. Geophys. Res.*
Atmos. 115. <https://doi.org/10.1029/2009JD013470>
- 650 Berrisford, P., Dee, D., Poli, P., Brugge, R., Fielding, K., Fuentes, M., Kallberg, P., Ko-
bayashi, S., Uppala, S., Simmons, A., 2009. The ERA-Interim Archive Version 2.0.
ERA Rep. Ser.
- Betts, A.K., Miller, M.J., 1986. A new convective adjustment scheme. Part II: Single
column tests using GATE wave, BOMEX, ATEX and arctic air-mass data sets. *Q. J.*
R. Meteorol. Soc. 112, 693–709. <https://doi.org/10.1002/qj.49711247308>
- 655 Bormann, K.J., Westra, S., Evans, J.P., McCabe, M.F., 2013. Spatial and temporal varia-
bility in seasonal snow density. *J. Hydrol.* 484, 63–73.
<https://doi.org/10.1016/j.jhydrol.2013.01.032>
- 660 Chen, F., Dudhia, J., 2001. Coupling an advanced land surface-hydrology model with the
Penn-State-NCAR MM5 modeling system. Part II: Preliminary model validation.
Mon. Weather Rev. 129, 587–604. [https://doi.org/10.1175/1520-
0493\(2001\)129<0587:CAALSH>2.0.CO;2](https://doi.org/10.1175/1520-0493(2001)129<0587:CAALSH>2.0.CO;2)
- Cluzet, B., Lafaysse, M., Cosme, E., Albergel, C., Meunier, L.-F., Dumont, M., 2020.
CrocO_v1.0 : a Particle Filter to assimilate snowpack observations in a spatialised
framework. *Geosci. Model Dev. Discuss.* 2020, 1–36. [https://doi.org/10.5194/gmd-
2020-130](https://doi.org/10.5194/gmd-2020-130)
- 665 Cook, B.I., Anchukaitis, K.J., Touchan, R., Meko, D.M., Cook, E.R., 2016. Spatiotem-
poral drought variability in the mediterranean over the last 900 years. *J. Geophys.*
Res. 121, 2060–2074. <https://doi.org/10.1002/2015JD023929>
- 670 Cortés, G., Giroto, M., Margulis, S., 2016. Snow process estimation over the extratropi-
cal Andes using a data assimilation framework integrating MERRA data and Land-
sat imagery. *Water Resour. Res.* 52, 2582–2600.
<https://doi.org/10.1002/2015WR018376>
- Dawson, N., Broxton, P., Zeng, X., 2017. A new snow density parameterization for land
data initialization. *J. Hydrometeorol.* 18, 197–207. [https://doi.org/10.1175/JHM-D-
16-0166.1](https://doi.org/10.1175/JHM-D-16-0166.1)

- 675 El-Fadel, M., Zeinati, M., Jamali, D., 2000. Water resources in Lebanon: Characterization, water balance and constraints. *Int. J. Water Resour. Dev.* 16, 615–638. <https://doi.org/10.1080/713672540>
- Essery, R., 2015. A factorial snowpack model (FSM 1.0). *Geosci. Model Dev.* 8, 3867–3876. <https://doi.org/10.5194/gmd-8-3867-2015>
- 680 Farajalla, N., Ziade, R., Bachour, R., 2011. Drought Frequency and Evapotranspiration Trends under a Changing Climate in the Eastern Mediterranean, in: *Water Scarcity and Policy in the Middle East and Mediterranean*. p. 11653. <https://doi.org/10.1002/aur.1388>
- Fayad, A., Gascoin, S., 2020. The role of liquid water percolation representation in estimating snow water equivalent in a Mediterranean mountain region (Mount Lebanon). *Hydrol. Earth Syst. Sci.* 24, 1527–1542. <https://doi.org/10.5194/hess-24-1527-2020>
- 685
- Fayad, A., Gascoin, S., Faour, G., Fanise, P., Drapeau, L., Somma, J., Fadel, A., Al Bitar, A., Escadafal, R., 2017a. Snow observations in Mount Lebanon (2011-2016). *Earth Syst. Sci. Data* 9, 573–587. <https://doi.org/10.5194/essd-9-573-2017>
- 690
- Fayad, A., Gascoin, S., Faour, G., López-Moreno, J.I., Drapeau, L., Page, M. Le, Escadafal, R., 2017b. Snow hydrology in Mediterranean mountain regions: A review. *J. Hydrol.* 551, 374–396. <https://doi.org/10.1016/j.jhydrol.2017.05.063>
- Fiddes, J., Aalstad, K., Westermann, S., 2019. Hyper-resolution ensemble-based snow reanalysis in mountain regions using clustering. *Hydrol. Earth Syst. Sci.* 23, 4717–4736. <https://doi.org/10.5194/hess-23-4717-2019>
- 695
- Fiddes, J., Gruber, S., 2014. TopoSCALE v.1.0: Downscaling gridded climate data in complex terrain. *Geosci. Model Dev.* 7, 387–405. <https://doi.org/10.5194/gmd-7-387-2014>
- 700
- García-Ruiz, J.M., López-Moreno, I.I., Vicente-Serrano, S.M., Lasanta-Martínez, T., Beguería, S., 2011. Mediterranean water resources in a global change scenario. *Earth-Science Rev.* 105, 121–139. <https://doi.org/10.1016/j.earscirev.2011.01.006>
- Gascoin, S., Grizonnet, M., Bouchet, M., Salgues, G., Hagolle, O., 2019. Theia Snow collection: High-resolution operational snow cover maps from Sentinel-2 and Landsat-8 data. *Earth Syst. Sci. Data* 11, 493–514. <https://doi.org/10.5194/essd-11-493-2019>
- 705

- Gascoin, S., Hagolle, O., Huc, M., Jarlan, L., Dejoux, J.F., Szczypta, C., Marti, R.,
Sánchez, R., 2015. A snow cover climatology for the Pyrenees from MODIS snow
products. *Hydrol. Earth Syst. Sci.* 19, 2337–2351. <https://doi.org/10.5194/hess-19-2337-2015>
710
- Gómez, B., Miguez-Macho, G., 2017. The impact of wave number selection and spin-up
time in spectral nudging. *Q. J. R. Meteorol. Soc.* 143, 1772–1786.
<https://doi.org/10.1002/qj.3032>
- Günther, D., Marke, T., Essery, R. and Strasser, U.: Uncertainties in Snowpack Simula-
tions—Assessing the Impact of Model Structure, Parameter Choice, and Forcing Da-
ta Error on Point-Scale Energy Balance Snow Model Performance, *Water Resour.*
715 *Res.*, 55(4), 2779–2800, doi:10.1029/2018WR023403, 2019.
- Gutmann, E., Barstad, I., Clark, M., Arnold, J., Rasmussen, R., 2016. The Intermediate
Complexity Atmospheric Research model (ICAR). *J. Hydrometeorol.* 17, 957–973.
720 <https://doi.org/10.1175/JHM-D-15-0155.1>
- Gutmann, E.D., Rasmussen, R.M., Liu, C., Ikeda, K., Gochis, D.J., Clark, M.P., Dudhia,
J., Thompson, G., 2012. A comparison of statistical and dynamical downscaling of
winter precipitation over complex terrain. *J. Clim.* 25, 262–281.
<https://doi.org/10.1175/2011JCLI4109.1>
- 725 Hall, D.K., Riggs, G.A., 2016. MODIS/Aqua Snow Cover Daily L3 Global 500m SIN
Grid, Version 6. NASA Natl. Snow Ice Data Cent. Distrib. Act. Arch. Center. Boul-
der, Color. USA. <https://doi.org/https://doi.org/10.5067/MODIS/MYD10A1.006>.
- Hall, D.K., Riggs, G.A., Salomonson, V. V, 2006. MODIS/Terra Snow Cover 8-day L3
Global 500m Grid V005. Color. USA Natl. Snow Ice Data Cent.
- 730 Harder, P., Pomeroy, J., 2013. Estimating precipitation phase using a psychrometric en-
ergy balance method. *Hydrol. Process.* 27, 1901–1914.
<https://doi.org/10.1002/hyp.9799>
- Herrero, J., Polo, M.J., Eugster, W., 2016. Evaposublimation from the snow in the Medi-
terranean mountains of Sierra Nevada (Spain). *Cryosphere* 10.
- 735 Hersbach, H., 2016. The ERA5 Atmospheric Reanalysis., in: Agufm. pp. NG33D-01.
- Horak, J., Hofer, M., Maussion, F., Gutmann, E., Gohm, A., Rotach, M.W., 2019. As-
sessing the added value of the Intermediate Complexity Atmospheric Research (IC-

AR) model for precipitation in complex topography. *Hydrol. Earth Syst. Sci.* 23, 2715–2734. <https://doi.org/10.5194/hess-23-2715-2019>

740 Ikeda, K., Rasmussen, R., Liu, C., Gochis, D., Yates, D., Chen, F., Tewari, M., Barlage, M., Dudhia, J., Miller, K., Arsenault, K., Grubišić, V., Thompson, G., Guttman, E., 2010. Simulation of seasonal snowfall over Colorado. *Atmos. Res.* 97, 462–477. <https://doi.org/10.1016/j.atmosres.2010.04.010>

745 Jaafar, H., Ahmad, F., Holtmeier, L., King-Okumu, C., 2020. Refugees, water balance, and water stress: Lessons learned from Lebanon. *Ambio* 49, 1179–1193. <https://doi.org/10.1007/s13280-019-01272-0>

Janjic, Z., 2002. Nonsingular Implementation of the Mellor-Yamada Level 2.5 Scheme in the NCEP Meso model. NCEP Off. Note 437, 61.

750 Janjic, Z.I., 1994. The step-mountain eta coordinate model: further developments of the convection, viscous sublayer, and turbulence closure schemes. *Mon. Weather Rev.* 122, 927–945. [https://doi.org/10.1175/1520-0493\(1994\)122<0927:TSMECM>2.0.CO;2](https://doi.org/10.1175/1520-0493(1994)122<0927:TSMECM>2.0.CO;2)

755 Jefferson, A.J., 2011. Seasonal versus transient snow and the elevation dependence of climate sensitivity in maritime mountainous regions. *Geophys. Res. Lett.* 38, n/a-n/a. <https://doi.org/10.1029/2011GL048346>

Jomaa, I., Saab, M.T.A., Skaf, S., El Haj, N., Massaad, R., 2019. Variability in Spatial Distribution of Precipitation Overall Rugged Topography of Lebanon, Using TRMM Images. *Atmos. Clim. Sci.* 09, 369–380. <https://doi.org/10.4236/acs.2019.93026>

760 Koeniger, P., Margane, A., Abi-Rizk, J., Himmelsbach, T., 2017. Stable isotope-based mean catchment altitudes of springs in the Lebanon Mountains. *Hydrol. Process.* 31, 3708–3718. <https://doi.org/10.1002/hyp.11291>

765 Kuribayashi, M., Noh, N.J., Saitoh, T.M., Tamagawa, I., Wakazuki, Y., Muraoka, H., 2013. Comparison of snow water equivalent estimated in central Japan by high-resolution simulations using different land-surface models. *Sci. Online Lett. Atmos.* 9, 148–152. <https://doi.org/10.2151/sola.2013-033>

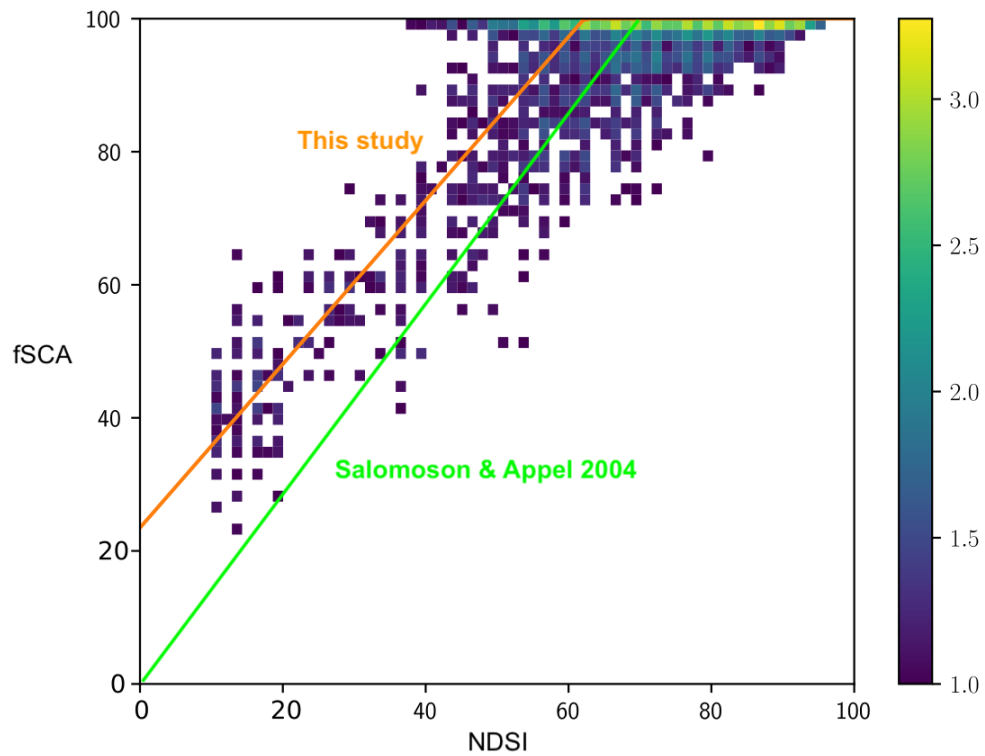
Legates, D., 2014. Climate models and their simulation of precipitation. *Energy Environ.* 25, 1163–1175. <https://doi.org/10.1260/0958-305X.25.6-7.1163>

- 770 Liston, G.E., 2004. Representing subgrid snow cover heterogeneities in regional and
global models. *J. Clim.* 17, 1381–1397. [https://doi.org/10.1175/1520-0442\(2004\)017<1381:RSSCHI>2.0.CO;2](https://doi.org/10.1175/1520-0442(2004)017<1381:RSSCHI>2.0.CO;2)
- Liston, G.E., Elder, K., 2006. A distributed snow-evolution modeling system (snowmodel). *J. Hydrometeorol.* 7, 1259–1276. <https://doi.org/10.1175/JHM548.1>
- 775 López-Moreno, J.I., Fassnacht, S.R., Beguería, S., Latron, J.B.P., 2011. Variability of
snow depth at the plot scale: Implications for mean depth estimation and sampling
strategies. *Cryosphere* 5, 617–629. <https://doi.org/10.5194/tc-5-617-2011>
- López-Moreno, J.I., García-Ruiz, J.M., 2004. Influence of snow accumulation and
snowmelt on streamflow in the central Spanish Pyrenees / Influence de
l'accumulation et de la fonte de la neige sur les écoulements dans les Pyrénées cen-
780 trales espagnoles. *Hydrol. Sci. J.* 49. <https://doi.org/10.1623/hysj.49.5.787.55135>
- López-Moreno, J.I., Gascoin, S., Herrero, J., Sproles, E.A., Pons, M., Alonso-González,
E., Hanich, L., Boudhar, A., Musselman, K.N., Molotch, N.P., Sickman, J., Pome-
roy, J., 2017. Different sensitivities of snowpacks to warming in Mediterranean cli-
mate mountain areas. *Environ. Res. Lett.* 12. [https://doi.org/10.1088/1748-](https://doi.org/10.1088/1748-9326/aa70cb)
785 [9326/aa70cb](https://doi.org/10.1088/1748-9326/aa70cb)
- Lundquist, J., Hughes, M., Gutmann, E., Kapnick, S., 2019. Our skill in modeling moun-
tain rain and snow is bypassing the skill of our observational networks. *Bull. Am.
Meteorol. Soc.* 100, 2473–2490. <https://doi.org/10.1175/BAMS-D-19-0001.1>
- 790 Margulis, S.A., Cortés, G., Giroto, M., Durand, M., 2016. A landsat-era Sierra Nevada
snow reanalysis (1985–2015). *J. Hydrometeorol.* 17, 1203–1221.
<https://doi.org/10.1175/JHM-D-15-0177.1>
- Margulis, S.A., Giroto, M., Cortés, G., Durand, M., 2015. A particle batch smoother
approach to snow water equivalent estimation. *J. Hydrometeorol.* 16, 1752–1772.
<https://doi.org/10.1175/JHM-D-14-0177.1>
- 795 Marty, C., Schögl, S., Bavay, M., Lehning, M., 2017. How much can we save? Impact of
different emission scenarios on future snow cover in the Alps. *Cryosphere* 11, 517–
529. <https://doi.org/10.5194/tc-11-517-2017>
- 800 Mernild, S.H., Liston, G.E., Hiemstra, C.A., Malmros, J.K., Yde, J.C., McPhee, J., 2017.
The Andes Cordillera. Part I: snow distribution, properties, and trends (1979–2014).
Int. J. Climatol. 37, 1680–1698. <https://doi.org/10.1002/joc.4804>

- Mhawej, M., Faour, G., Fayad, A., Shaban, A., 2014. Towards an enhanced method to map snow cover areas and derive snow-water equivalent in Lebanon. *J. Hydrol.* 513, 274–282. <https://doi.org/10.1016/j.jhydrol.2014.03.058>
- 805 Montavez, J.P., Lopez-Romero, J.M., Jerez, S., Gomez-Navarro, J.J., Jimenez-Guerrero, P., 2017. How much spin-up period is really necessary in regional climate simulations?, in: *Geophysical Research Abstracts EGU General Assembly*. Vienna, Austria, pp. 2017–15806.
- Nappo, C.J., 2012. *The Linear Theory*, 2nd ed, International Geophysics. Academic Press. <https://doi.org/10.1016/B978-0-12-385223-6.00002-1>
- 810 Neale, R.B., Chen, C., Lauritzen, P.H., Williamson, D.L., Conley, A.J., Smith, A.K., Mills, M., Morrison, H., 2004. Description of the NCAR Community Atmosphere Model (CAM 5.0). *Ncar/Tn-464+Str* 214. <https://doi.org/10.5065/D63N21CH>
- 815 Niu, G.Y., Yang, Z.L., Mitchell, K.E., Chen, F., Ek, M.B., Barlage, M., Kumar, A., Manning, K., Niyogi, D., Rosero, E., Tewari, M., Xia, Y., 2011. The community Noah land surface model with multiparameterization options (Noah-MP): 1. Model description and evaluation with local-scale measurements. *J. Geophys. Res. Atmos.* 116, D12109. <https://doi.org/10.1029/2010JD015139>
- 820 Peel, M.C., Finlayson, B.L., McMahon, T.A., 2007. Updated world map of the Köppen-Geiger climate classification. *Hydrol. Earth Syst. Sci.* 11, 1633–1644. <https://doi.org/10.5194/hess-11-1633-2007>
- 825 Rasmussen, R., Liu, C., Ikeda, K., Gochis, D., Yates, D., Chen, F., Tewari, M., Barlage, M., Dudhia, J., Yu, W., Miller, K., Arsenault, K., Grubišić, V., Thompson, G., Gutmann, E., 2011. High-resolution coupled climate runoff simulations of seasonal snowfall over Colorado: A process study of current and warmer climate. *J. Clim.* 24, 3015–3048. <https://doi.org/10.1175/2010JCLI3985.1>
- Saavedra, F.A., Kampf, S.K., Fassnacht, S.R., Sibold, J.S., 2017. A snow climatology of the Andes Mountains from MODIS snow cover data. *Int. J. Climatol.* 37, 1526–1539.
- 830 Salomonson, V. V., Appel, I., 2004. Estimating fractional snow cover from MODIS using the normalized difference snow index. *Remote Sens. Environ.* 89, 351–360. <https://doi.org/10.1016/j.rse.2003.10.016>

- Schulz, O., de Jong, C., 2004. Snowmelt and sublimation: field experiments and modeling in the High Atlas Mountains of Morocco. *Hydrol. Earth Syst. Sci.* 8, 1076–1089. <https://doi.org/10.5194/hess-8-1076-2004>
- 835 Skamarock, W.C., Klemp, J.B., Dudhia, J.B., Gill, D.O., Barker, D.M., Duda, M.G., Huang, X.-Y., Wang, W., Powers, J.G., 2008. A description of the Advanced Research WRF Version 3, NCAR Technical Note TN-475+STR. Tech. Rep. 113. <https://doi.org/10.5065/D68S4MVH>
- 840 Smolarkiewicz, P.K., Margolin, L.G., 1998. MPDATA: A Finite-Difference Solver for Geophysical Flows. *J. Comput. Phys.* <https://doi.org/10.1006/jcph.1998.5901>
- Sproles, E.A., Nolin, A.W., Rittger, K., Painter, T.H., 2013. Climate change impacts on maritime mountain snowpack in the Oregon Cascades. *Hydrol. Earth Syst. Sci.* 17, 2581–2597. <https://doi.org/10.5194/hess-17-2581-2013>
- 845 Suzuki, K., Zupanski, M., 2018. Uncertainty in solid precipitation and snow depth prediction for Siberia using the Noah and Noah-MP land surface models. *Front. Earth Sci.* 12, 672–682. <https://doi.org/10.1007/s11707-018-0691-2>
- Tarek, M., Brissette, F., Arsenault, R., 2019. Evaluation of the ERA5 reanalysis as a potential reference dataset for hydrological modeling over North-America. *Hydrol. Earth Syst. Sci. Discuss.* 2019, 1–35. <https://doi.org/10.5194/hess-2019-316>
- 850 Telesca, L., Shaban, A., Gascoin, S., Darwich, T., Drapeau, L., Hage, M. El, Faour, G., 2014. Characterization of the time dynamics of monthly satellite snow cover data on Mountain Chains in Lebanon. *J. Hydrol.* 519, 3214–3222. <https://doi.org/10.1016/j.jhydrol.2014.10.037>
- 855 Thompson, G., Field, P.R., Rasmussen, R.M., Hall, W.D., 2008. Explicit forecasts of winter precipitation using an improved bulk microphysics scheme. Part II: Implementation of a new snow parameterization. *Mon. Weather Rev.* 136, 5095–5115. <https://doi.org/10.1175/2008MWR2387.1>
- Van Leeuwen, P.J., 2009. Particle filtering in geophysical systems. *Mon. Weather Rev.* 137, 4089–4114. <https://doi.org/10.1175/2009MWR2835.1>
- 860 van Pelt, W.J.J., Kohler, J., Liston, G.E., Hagen, J.O., Luks, B., Reijmer, C.H., Pohjola, V.A., 2016. Multidecadal climate and seasonal snow conditions in Svalbard. *J. Geophys. Res. Earth Surf.* 121, 2100–2117. <https://doi.org/10.1002/2016JF003999>

- Verseghy, D.L., 1991. Class—A Canadian land surface scheme for GCMS. I. Soil model. *Int. J. Climatol.* 11, 111–133. <https://doi.org/10.1002/joc.3370110202>
- 865 Viviroli, D., Dürr, H.H., Messerli, B., Meybeck, M., Weingartner, R., 2007. Mountains of the world, water towers for humanity: Typology, mapping, and global significance. *Water Resour. Res.* 43. <https://doi.org/10.1029/2006WR005653>
- Von Storch, H., Langenberg, H., Feser, F., 2000. A spectral nudging technique for dynamical downscaling purposes. *Mon. Weather Rev.* 128, 3664–3673.
- 870 [https://doi.org/10.1175/1520-0493\(2000\)128<3664:ASNTFD>2.0.CO;2](https://doi.org/10.1175/1520-0493(2000)128<3664:ASNTFD>2.0.CO;2)
- Waldron, K.M., Paegle, J., Horel, J.D., 1996. Sensitivity of a spectrally filtered and nudged limited-area model to outer model options. *Mon. Weather Rev.* 124, 529–547. [https://doi.org/10.1175/1520-0493\(1996\)124<0529:SOASFA>2.0.CO;2](https://doi.org/10.1175/1520-0493(1996)124<0529:SOASFA>2.0.CO;2)
- Wang, C., Graham, R.M., Wang, K., Gerland, S., Granskog, M.A., 2019. Comparison of
875 ERA5 and ERA-Interim near-surface air temperature, snowfall and precipitation over Arctic sea ice: effects on sea ice thermodynamics and evolution. *Cryosphere* 13, 1661–1679. <https://doi.org/10.5194/tc-13-1661-2019>
- Wang, D., Morton, D., Masek, J., Wu, A., Nagol, J., Xiong, X., Levy, R., Vermote, E.,
880 Wolfe, R., 2012. Impact of sensor degradation on the MODIS NDVI time series. *Remote Sens. Environ.* 119, 55–61. <https://doi.org/10.1016/J.RSE.2011.12.001>
- Wegmann, M., Orsolini, Y., Dutra, E., Bulygina, O., Sterin, A., Brönnimann, S., 2017. Eurasian snow depth in long-term climate reanalyses. *Cryosphere* 11, 923–935. <https://doi.org/10.5194/tc-11-923-2017>
- Wu, X., Che, T., Li, X., Wang, N., Yang, X., 2018. Slower Snowmelt in Spring Along
885 With Climate Warming Across the Northern Hemisphere. *Geophys. Res. Lett.* 45, 12,331–12,339. <https://doi.org/10.1029/2018GL079511>
- Yilmaz, Y., Aalstad, K., Sen, O., 2019. Multiple Remotely Sensed Lines of Evidence for a Depleting Seasonal Snowpack in the Near East. *Remote Sens.* 11, 483. <https://doi.org/10.3390/rs11050483>



Supplementary 1: Comparison of Salomoson and Appel 2004 function and the newly developed linear equation. The color scale represents the logarithmic relative density by bins.